Resource Allocation for Cooperative Transmission in Optical Wireless Cellular Networks with Illumination Requirements

Borja Genovés Guzmán, *Student Member, IEEE,* Alexis A. Dowhuszko, *Senior Member, IEEE,* Víctor P. Gil Jiménez, *Senior Member, IEEE,* and Ana I. Pérez-Neira, *Senior Member, IEEE*

***Abstract*—Visible light communication (VLC) often suffers from line-of-sight path blockages and high levels of inter-cell interference. Thus, the analysis and design of cooperation techniques become crucial to address these key impairments. This paper studies the performance of different resource allocation schemes that are suitable for multi-cell cooperative transmission when tri- and tetra-chromatic light-emitting diodes (LEDs) and optical orthogonal frequency-division multiple access are utilized. Firstly, guidelines are derived for maintaining the same spatial distribution of the signal-to-interference-plus-noise ratio (SINR) in every sector of the multi-cell environment in case of stand-alone (non-cooperative) and cooperative transmission. Secondly, the possible resource allocation configurations for both stand-alone and cooperative transmission modes are identified for different LED types and available orthogonal resources (*i.e.*, frequency sub-bands per color and sectors per cell). Finally, the data rate gain of the multiple resource allocation configurations are also analyzed, while verifying the illumination constraints. The obtained results confirm that the proper design of cooperative transmission configurations will be of paramount importance to provide reliable wireless link in ultra-dense VLC deployments.**

***Index Terms*—Coordinated multi-point, illumination requirements, joint transmission, line-of-sight blockage, multi-color LED, resource allocation, ultra-dense deployments, visible light communication.**

I. Introduction

THE radio frequency (RF) spectrum is becoming overcrowded owing to the increasing demand of wireless communication services [1] and, due to that, the research and development community is searching for new alternatives to satisfy the foreseen traffic demands. Visible light communication (VLC) has lately emerged as a novel solution [2] to prevent the RF spectrum crunch, as it uses the large available bandwidth in the optical (license-free) portion of the electromagnetic spectrum. In addition, VLC takes advantage of the fast time response of light-emitting diodes (LEDs) and photodiodes (PDs), which enables the transmission of wide-band electrical waveforms. Intensity modulation (IM) schemes are utilized in the transmitter because the LED is a non-coherent source of light. In the receiver, direct detection (DD) is performed by a PD that senses the instantaneous intensity of the received optical signal and converts it into an electrical current. Solid-state lighting has notably evolved during last years, and LED lamps have been replacing gradually other lighting technologies based on incandescent, fluorescent and/or halogen lamps. Thus, the required infrastructure for VLC is already present, to facilitate the deployment of the technology to enable wireless access and lighting services simultaneously.

VLC networks are being developed to provide a seamless coverage indoors [3] [4]. In this context, performance analysis in multi-cell VLC networks is more critical than in single-cell scenarios, due to the impact that inter-cell interference has in actual settings. Multi-cell VLC networks, also known as attocell networks [5], suffer from high inter-cell interference due to the necessity of complying with the stringent lighting regulations that exist in terms of mean illumination and illumination uniformity, which imply the deployment of multiple light fixtures in the same room. Thus, inter-cell interference mitigation techniques become essential to keep this impairment under control. Besides, when working with visible light wavelengths, line-of-sight (LoS) blockage notably impacts the achievable data rate on the VLC link. This is because most received signal power is collected from the LoS path; therefore, when the LoS link is blocked, the received signal strength decreases several tens of dB [6]. In this case, when there is a non-line-of-sight (NLoS) condition between the transmitter and the receiver, most VLC users become in outage, particularly in presence of strong interference coming from adjacent cells.

Different techniques have been proposed in the literature to mitigate the strong inter-cell interference that multi-cell VLC systems experience in cell-edge areas. For example, fractional frequency reuse (FFR) utilizes different frequency-reuse factors in cell-center and cell-edge areas. This way, the authors of [7] and [8] evaluated FFR in VLC scenarios, showing a considerable inter-cell interference reduction for those users located on the borders of the cells. However, in ultra-dense VLC networks, even users located in the center of the cells – just below the light fixtures – also suffer from notable inter-cell interference power coming from adjacent lamps.

Similarly, joint transmission (JT) coordinated multi-point (CoMP) can also be employed in multi-cell VLC systems to convert inter-cell interference – coming from adjacent transmission points – into useful signal [9]–[11]. Early studies on frequency allocation for CoMP were made in [5], seeking

B. Genovés Guzmán is with IMDEA Networks Institute. Alexis A. Dowhuszko is with the Department of Communications and Networking, School of Electrical Engineering, Aalto University. Víctor P. Gil Jiménez is with the Department of Signal Theory and Communications of the University Carlos III of Madrid. Ana I. Pérez-Neira is with the Centre Tecnològic de Telecomunicacions de Catalunya (CTTC/CERCA). Email: borja.genoves@imdea.org; alexis.dowhuszko@aalto.fi; vgil@tsc.uc3m.es; ana.perez@cttc.es.

the data rate improvement for cell-edge users when the access points (APs) were equipped with directional LEDs pointing to the cell edges. In addition to inter-cell interference mitigation, JT-CoMP has also been proposed to combat the LoS blockage problem that VLC technology experiences [12], [13]. Moreover, the authors of [14] proposed to use CoMP to enable smoother handover operations among adjacent VLC APs, and the authors of [4], [15] combined CoMP with spatial-division multiple access (SDMA) to implement a pre-coded transmission to different groups of users that are clustered *a priori*. Although the use of CoMP in VLC has demonstrated a better communication reliability than in a single-point transmission, most of the techniques proposed so far are optimized for the specific set of active users, with an implementation complexity that grows exponentially with the number of candidates. Furthermore, these solutions are not static, making the communication unstable and unreliable when LoS blockages with relative short duration happen regularly (e.g., when obstacles pass by quickly). Note that these techniques must sense the optical wireless channel continuously and reallocate resources accordingly if a blockage event is detected; in addition, since the blockage also affects the feedback channel, the user would not have the chance to timely inform about this situation to the serving AP. Thus, it is desirable that the resource allocation scheme of the multi-cell VLC system is pre-defined, to give as homogeneous signal-to-interference-plus-noise ratio (SINR) as possible in the whole coverage area.

When focusing on static resource allocation approaches, the authors of [16] and [17] studied the performance of pre-defined cooperative transmission schemes using phosphor-converted LEDs with on-off-keying (OOK) and optical orthogonal frequency division multiplexing (O-OFDM), respectively. However, both references studied the achievable data rate for a specific JT-CoMP scheme. In this paper, red-green-blue(-yellow) RGB(Y) LED technology is used instead, enabling more flexibility by using wavelength division multiplexing (WDM). In line with this, a preliminary study was presented in [18], where only one specific cooperative scheme was evaluated. However, in this paper we present a generalization of the resource allocation scheme that was introduced, where the illumination requirements to be fulfilled are also characterized in detail.

In this paper we state the conditions to be verified when allocating resources for cooperative multi-point transmission in a VLC multi-cell network that aims at giving the same spatial SINR distribution regardless of the specific cell/sector in which the user is placed. As a consequence, a homogeneous quality of service can be provided in the whole coverage area, and reliable cooperative transmission schemes that do not need to continuously sense the status of the optical wireless channel can be implemented. Thanks to the cooperative multi-point transmission, two key drawbacks in VLC networks are tackled, namely the effect of strong inter-cell interference and the impact of frequent LoS-link blockage. This way, we also address the problem that low-cost Internet of Things (IoT) devices have for sensing the status of the optical channel [19], since a good quality link to the serving APs will likely be present as illustrated in Fig. 1, even in presence of quick harmful LoS blockages. On the other hand, we thoroughly study all the possible VLC resource-reuse patterns for cooperative transmission, and determine the most convenient schemes for the given working conditions.

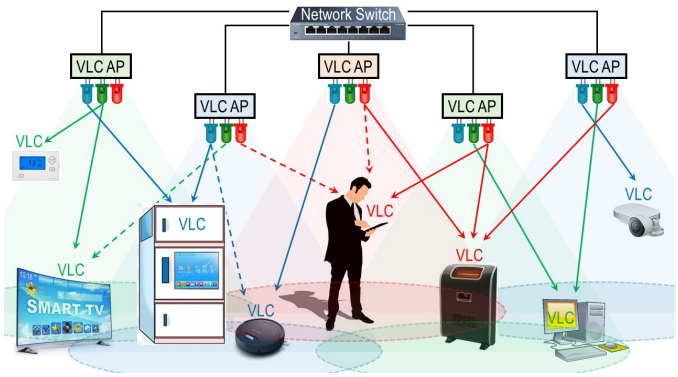

Fig. 1: Representation of an IoT scenario using VLC technology. LoS links to cooperative VLC APs are represented with solid lines, whereas blocked VLC links are shown with dashed lines. Different colors identify the communication resource that is utilized for serving users located in each cell/sector of the VLC network.

The rest of the paper is structured as follows: Section II discusses the system model, presents the key definitions, and specifies the illumination requirements. Section III introduces the homogeneity concept in a multi-cell network setting, as well as the statements that should be verified to achieve it in a practical configuration. Section IV carries out the SINR and data rate performance analysis for the different resource allocation schemes, as well as the verification of the illumination requirements in each case. Finally, conclusions are drawn in Section V.

II. System Model

Optical OFDM-based transmission schemes and RGB(Y) LEDs [20] [21] are used in this paper to achieve higher data rates in a multi-cell VLC scenario, such as the one illustrated in Fig. 1. Note that the multi-cell VLC network is deployed in a large room without walls or large objects. The area of each cell is approximated by a hexagon whose HEX radius is $\widetilde{R} \approx 1.1R$ [22], where R is the corresponding equal-area circular cell radius as represented in Fig. 2a. Cells are divided into $|\mathcal{S}|$ sectors for different configurations, where $s \in \mathcal{S}$ is the index of each sector in the cell. Note that the sectors are logical divisions, as a single RGB(Y) LED with Lambertian radiation pattern is placed in the center of each cell. Therefore, the number of orthogonal resources that can be allocated in the different sectors of the multi-cell VLC network is given by

$$N = |\mathcal{T}| \cdot |\mathcal{F}| \cdot |\mathcal{C}|, \tag{1}$$

where $|\mathcal{T}|$ is the number of orthogonal time slots, $|\mathcal{F}|$ is the number of orthogonal frequency sub-bands in the electrical signal that modulates the intensity of each LED color, and $|\mathcal{C}|$ is the number of LED chip colors used for generating the white light. In [17], the authors proposed a robust cooperative transmission scheme relying on time-domain multiple access for serving users located in different sectors, at the expense of

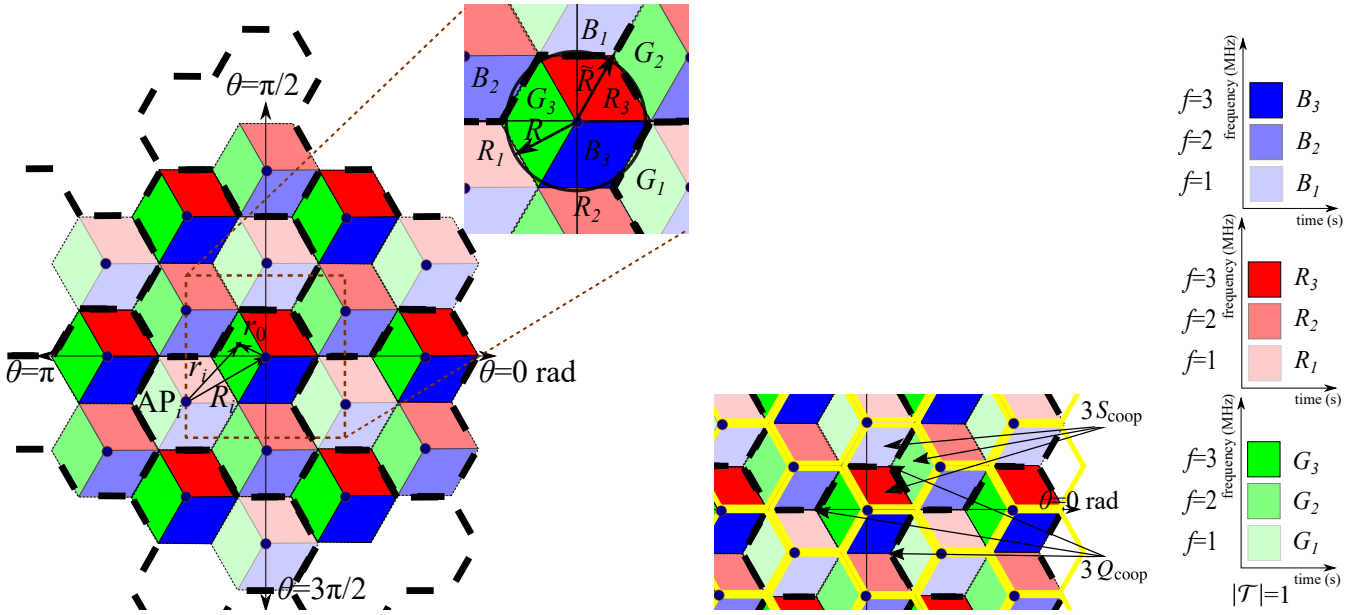

(a) Resource allocation scheme suitable for single-cell transmission. Dashed black lines represent cell clusters ($Q_0 = 3$).

(b) Cooperation strategy with $M = 3$ APs per cooperating area (solid yellow lines).

(c) Orthogonal resources.

Fig. 2: Sample resource allocation for a multi-cell VLC network with RGB LEDs ($|C|$=3), three sectors per cell ($|\mathcal{S}|$=3), and three electrical frequency sub-bands per color ($|\mathcal{F}|$=3). Cell clusters and cooperative sets are shown.

reducing the system mean data rate. Therefore, in this paper we do not use time-domain multiple access ($|\mathcal{T}| = 1$), simplifying (1) to $N = |\mathcal{F}| \cdot |C|$.

Cells can be grouped into clusters, defined as sets of adjacent cells that use orthogonal communication resources and, together, utilize the N resources available in the VLC system. Therefore, the cluster size is given by

$$Q_0 = \frac{N}{|\mathcal{S}|} = \frac{|C| \cdot |\mathcal{F}|}{|\mathcal{S}|}. \quad (2)$$

As an example, Fig. 2 shows the way in which orthogonal communication resources can be assigned in a two-tier multi-cell network, where RGB LEDs are utilized ($|C| = 3$), cells are divided into three sectors ($|\mathcal{S}| = 3$), and the electrical bandwidth per color is split into $|\mathcal{F}| = 3$ sub-bands represented with different levels of brightness. Thus, the number of available resources is $N = 9$, and the cluster size without cooperation is $Q_0 = 3$ (black dashed lines in Fig. 2a).

Cooperative transmission among groups of APs can reduce the outage probability due to blockage, and mitigate the inter-cell interference power that would otherwise come from these adjacent APs if not cooperating. The number of APs that cooperate in transmission at every location is denoted by M, and the sector/cell tessellation is arranged into cooperation sets as shown with yellow solid lines in Fig. 2b. Users that are placed inside the service area of these cooperation sets are jointly served by the nearest APs. To further characterize the possible cooperative transmission configurations, two new parameters shown in Fig. 2b are defined:

- S_{coop}: Number of sectors within a cooperation area.
- Q_{coop}: Number of cooperation areas in which an AP cooperates.

Taking into account both the cooperation and sectorization strategies, a final cluster Q that contains all the possible resources combined with all the sectorization modes will be defined. To facilitate the reading of this paper, Table I summarizes the symbol terminology that is used.

TABLE I: Terminology that defines the resource allocation configuration in (non-)cooperative multi-cell transmission.

Variable	Description
$\|C\|$	Number of chip colors per LED
$\|\mathcal{F}\|$	Number of electrical sub-bands per color
$\|\mathcal{S}\|$	Number of sectors per cell
N	Number of orthogonal communication resources
Q_0	Cell cluster size without cooperation
Q	Cell cluster size with cooperation
M	Number of APs that cooperate at every location
S_{coop}	Number of sectors within a cooperation area
Q_{coop}	Number of cooperation areas in which every AP cooperates
W	Electrical bandwidth of the LED chip

A. Overview of the VLC link based on Optical OFDM

The block diagram of the VLC system that is used in this paper is presented in Fig. 3 and consists of a transmitter, an optical wireless channel, and a receiver. Though the analysis that is presented can be adapted for the different O-OFDM schemes reported in the literature so far [23] (*e.g.*, by adapting the achievable data rate formulas that are derived), this paper focuses on direct-current biased Optical OFDM (DCO-OFDM) for the sake of brevity. On the transmitter side, the stream of input bits is distributed among the three (four) independent transmission chains that correspond to each of the colors of the RGB (RGBY) LED technology. Let $c \in C$ be the color index for a given bit stream, such that

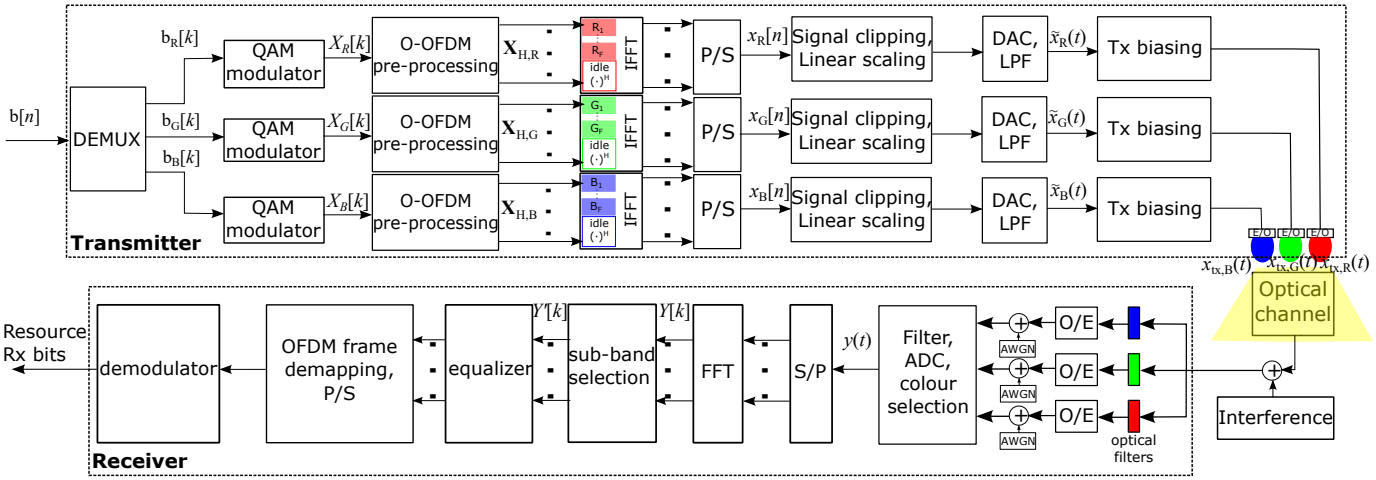

Fig. 3: Block diagram of a VLC link-level transmission using DCO-OFDM modulation with a RGB LED.

$C = \{R, G, B\}$ ($C = \{R, G, B, Y\}$) for a RGB (RGBY) LED. Once the bits for each color are mapped into quadrature amplitude modulated (QAM) symbols, a pre-processing is performed to generate blocks of symbols of size K that verify the Hermitian symmetry property needed to obtain a real-valued signal at the output of the inverse fast Fourier transform (IFFT) block. Besides, the subcarriers with indices 0 and $K/2$ are zero-valued in DCO-OFDM. Thus, the frequency-domain (FD) signal for color c becomes

$$\mathbf{X}_{\mathrm{H},c} = \left[0 \;\; \{X_c[k]\}_{k=1}^{K/2-1} \;\; 0 \;\; \{X_c[K/2-k]^*\}_{k=1}^{K/2-1}\right], \quad c \in C, \tag{3}$$

where $X_c[k]$ is the symbol transmitted on the k-th subcarrier by the color chip c and $(\cdot)^*$ denotes the complex conjugate. The time-domain (TD) real-valued signals at the output of the IFFT blocks are denoted as $x_{\mathrm{R}}[n]$, $x_{\mathrm{G}}[n]$ and $x_{\mathrm{B}}[n]$, respectively. Note that $|\mathcal{F}|$ frequency sub-bands are defined for each color to increase the degrees of freedom that are available to perform the resource allocation. The TD signals must be DC-shifted and scaled according to the dynamic range of the electrical signal that drives the LED chip, taking into account that the effect of the added clipping noise becomes negligible with respect to the optical interference and ambient background noise [24]. Then, the transmitted optical signals for each color c attains the form

$$x_{\mathrm{tx},c}(t) = \int_{\lambda} S_c(t,\lambda)\mathrm{d}\lambda = \; \eta_{\mathrm{led},c}\left(\tilde{x}_c(t) + I_{\mathrm{dc},c}\right), \quad c \in C, \tag{4}$$

where $S_c(t,\lambda)$ is the time-varying optical spectral power density of the LED chip c at wavelength λ, $\eta_{\mathrm{led},c}$ is the electrical-to-optical conversion efficiency for the corresponding LED chip, and $\tilde{x}_c(t) = \sigma_{\mathrm{x},c} \cdot x_c(t)$ is the scaled version of the TD signal before DC-shift. Note that $\sigma_{\mathrm{x},c}$ is the scaling factor for the Gaussian-like OFDM signal, whereas $I_{\mathrm{dc},c}$ is the DC component that is added in order to comply with the target white chromaticity and illumination level requirements.

On the receiver side, a white light is received and filtered through three (or four) optical filters to recover the streams of bits that are independently transmitted over the different colors. Then, each user demodulates the sub-band of the electrical signal that is transported on the optical color that corresponds to the sector in which it is located. Note that a simplified positioning system sensing either downlink signals (i.e., user estimates the sector in which it is placed measuring the received power coming from the nearest APs) or the uplink signal (i.e., clusters of adjacent APs measure and identify jointly the sector in which the user is placed based on the infrared/radio signal strength that is received) is required [25]. The wideband electrical signal at the output of the PD, which should be demultiplexed to recover the frequency sub-band of the sector, is given by

$$y(t) = \int_{\lambda} \eta_{\mathrm{pd},c}(\lambda) \left(\sum_{i \in \mathcal{D}} S_{i,c}(t,\lambda) \circledast h_i(t,\lambda) + \sum_{i \in \mathcal{I}} S_{i,c}(t,\lambda) \circledast h_i(t,\lambda) \right) \mathrm{d}\lambda + n_{\mathrm{rx},c}(t), \quad c \in C, \tag{5}$$

where $\mathcal{D}$ and $\mathcal{I}$ are the set with the indexes of cooperating (Desired) and interfering APs, respectively, whereas $\eta_{\mathrm{pd}}(\lambda)$ is the spectral responsivity of the PD and $h_i(t,\lambda)$ is the optical wireless channel impulse response (CIR) at wavelength λ from the i-th AP to the user under study. Note that $h_i(t,\lambda)$ also takes into account any wavelength-selective behaviour introduced by the hardware components of the VLC system, such as the optical filters whose actual spectral transmittance varies with the angle of incidence of the light beam.

To simplify the analysis, the PD responsivity for a given color c can be modeled as wavelength-independent [20] using $\eta_{\mathrm{pd},c} = \int_{\lambda} \eta_{\mathrm{pd}}(\lambda) \cdot S_{\mathrm{f},c}(\lambda)\mathrm{d}\lambda \,/\, \int_{\lambda} S_{\mathrm{f},c}(\lambda)\mathrm{d}\lambda$, where $S_{\mathrm{f},c}(\lambda)$ is the optical power spectrum at the output of the optical filter, whose passband fits with the monochromatic optical spectrum that the target LED chip generates. Though $\eta_{\mathrm{pd},c}$ is an approximation of $\eta_{\mathrm{pd}}(\lambda)$, the reality is that either of them will affect in the same way the spectral power density of both desired signal and interference. Thus, any minor variation on the responsivity becomes negligible when assessing the performance of a multi-cell scenario that is limited by interference rather than noise as it will be seen in Section IV (i.e., SINR approximates signal-to-interference power ratio very well). Similarly, it is also assumed that h_i is wavelength independent, as the dominant

interference power coming from nearest APs will have a very similar angle of incidence, which means a negligible variation in the transmitance of optical filter [26]. Thus, (5) may be simplified as

$$y(t)=\eta_{\text{pd}}\eta_{\text{led},c}\left(\sum_{i\in\mathcal{D}}(\tilde{x}_{i,c}(t)+I_{\text{dc},c})\circledast h_i(t)+\sum_{i\in\mathcal{I}}(\tilde{x}_{i,c}(t)+I_{\text{dc},c})\circledast h_i(t)\right) +n_{\text{rx},c}(t), \quad c\in C. \tag{6}$$

Furthermore, $n_{\text{rx},c}(t)$ is the zero-mean additive white Gaussian noise (AWGN) with variance

$$\sigma^2_{\text{rx},c}=\frac{N_{0,c}2W}{|\mathcal{F}|\xi^2}, \quad c\in C, \tag{7}$$

where $N_{0,c}$ is the noise power spectral density for color c, W is the electrical bandwidth of the LED, and $\xi=\sqrt{K/(K-2)}$ is a normalizing factor to compensate the zero-power in the 0-th and $N/2$-th subcarriers of the DCO-OFDM waveform. The factor of 2 in the numerator of (7) comes from the whole modulation bandwidth of the baseband electrical signal. Note that noise power is divided by $|\mathcal{F}|$ since the received signal in a sector occupies only one sub-band. The noise power spectral density for color c includes shot and thermal noise, and is defined as

$$\begin{aligned}N_{0,c}&=N_{0,\text{s},c}+N_{0,\text{th}}\\&=2q\eta_{\text{pd}}\left(\sum_i P_{\text{opt},c}H_i+E_{\text{r,ab}}A_{\text{pd}}\right)+\frac{4\kappa_{\text{B}}T_{\text{abs}}}{R_{\text{L}}}, \quad c\in C,\end{aligned} \tag{8}$$

where $q=1.6\cdot10^{-19}$ C is the electron charge, and $\sum_i P_{\text{opt},c}H_i$ represents the total optical power received for color c, where $H_i=FT\{h_i(t)\}$ is the FD channel transfer function from the i-th AP to the user under study. In addition, $E_{\text{r,ab}}$ is the incident irradiance of the ambient light, A_{pd} represents the physical area of the PD, $\kappa_{\text{B}}=1.38\cdot10^{-23}$ J/K is the Boltzmann constant, T_{abs} denotes the absolute temperature, and R_{L} is the equivalent load resistance of the receiver circuit.

The FD received signal on subcarrier k can be represented as

$$Y[k]=\eta_{\text{pd}}\eta_{\text{led},c}\left(\sum_{i\in\mathcal{D}}\tilde{X}_{i,c}[k]H_i+\sum_{i\in\mathcal{I}}\tilde{X}_{i,c}[k]H_i\right)+N_{\text{rx},c}[k], \quad c\in C, \tag{9}$$

where $\tilde{X}_{i,c}[k]$ is the QAM symbol transported on the k-th subcarrier of color c from AP with index i (after the TD clipping and amplification), and $N_{\text{rx},c}[k]$ is the equivalent FD noise in reception. The FD channel transfer function from the i-th AP is assumed flat [26], i.e.,

$$H_i=\begin{cases}\frac{A_{\text{pd}}(m+1)}{2\pi\left(r_i^2+d_{\text{v}}^2\right)}\cos^m(\phi_i)\cos(\psi_i)=\frac{A_{\text{pd}}(m+1)d_{\text{v}}^{m+1}}{2\pi\left(r_i^2+d_{\text{v}}^2\right)^{\frac{m+3}{2}}} & \psi_i\le\Psi_{\max}\\ 0 & \psi_i>\Psi_{\max}\end{cases} \tag{10}$$

where ψ_i is the angle of incidence and $\Psi_{\max}$ is the field of view (FOV) of the PD. The radiance angle between AP i and user is denoted by ϕ_i, whereas d_{v} is the vertical separation between AP and PD, and $m=-1/\log_2\left(\cos(\phi_{1/2})\right)$ is the Lambertian emission order [27] that depends on the LED half-power semi-angle $\phi_{1/2}$. The horizontal distance with the i-th AP is denoted by r_i (see Fig. 2a). Let us assume that (r_0,θ) are the polar coordinates of the user's location with respect to the central AP. Then, the distance between this user and the AP with index i is

$$r_i(r_0,\theta)=\sqrt{r_0^2+R_i^2-2R_ir_0\cos(\theta-\Theta_i)} \tag{11}$$

where (R_i,Θ_i) represents the location of AP i in polar coordinates (see Fig. 2a). Note that the NLoS component of the CIR is neglected in this study, as its effect would be minimal due to the high probability of having strong LoS link(s) when implementing multi-point transmission.

Throughout this paper, we assume that the direction of the light beam that the APs emit is perfectly vertical, with a boresight direction of its optical spatial power distribution pointing directly to the floor. Similarly, it is considered that the direction of the axis of the PD reception cone is also vertical, pointing perfectly upwards towards the ceiling of the room.

Based on (4), the optical power that each LED chip c transmits is given by

$$\begin{aligned}P_{\text{opt},c}=\text{E}\left\{x_{\text{tx},c}(t)\right\}&=\eta_{\text{led},c}\ \left(\text{E}\left\{\tilde{x}_c(t)\right\}+I_{\text{dc},c}\right),\\&=\eta_{\text{led},c}\,\sigma_{\text{x},c}\ \left(\text{E}\left\{x_c(t)\right\}+\zeta_c\right), \quad c\in C,\end{aligned} \tag{12}$$

where $\text{E}\{\cdot\}$ represents the statistical expectation and $\zeta_c=\frac{I_{\text{dc},c}}{\sigma_{\text{x},c}}$ is the ratio of DC-bias level to the standard deviation of the transmitted electrical signal [28]. Assuming that $\text{E}\{x_c(t)\}\approx0$, and that the total optical power that a multi-color LED transmits is equally divided among the color chips used for generating the white light, the electrical transmit signal power becomes

$$\sigma^2_{x,c}=\sigma^2_x=\left(\frac{P_{\text{opt}}}{|C|\,\eta_{\text{led}}\,\zeta}\right)^2, \quad c\in C. \tag{13}$$

B. Figures of merit

The SINR, which is needed to evaluate the data rate of a communication link, is given by

$$\Gamma_c=\frac{\sum_{i\in\mathcal{D}}D_i}{\sum_{i\in\mathcal{I}}I_i+\sigma^2_{\text{rx}}}=\frac{\frac{1}{\nu}\eta^2_{\text{pd}}\eta^2_{\text{led}}\sigma^2_{\text{x}}\xi^2\left|\sum_{i\in\mathcal{D}}H_i\right|^2}{\frac{1}{\nu}\eta^2_{\text{pd}}\eta^2_{\text{led}}\sigma^2_{\text{x}}\xi^2\sum_{i\in\mathcal{I}}|H_i|^2+\sigma^2_{\text{rx}}}, \quad c\in C, \tag{14}$$

where ν is the number of frequency sub-bands in color c that are active in each AP, and D_i and I_i describe the received signal power coming from the serving (Desired) and interfering APs, respectively. Without loss of generality, the noise power is assumed identical for all colors. Then, combining (10) and (13) into (14), and setting the FOV angle $\Psi_{\max}=90°$ (i.e., worst case from optical interference perspective as users receive optical signal from all APs), the SINR becomes

$$\Gamma(r_0,\theta)=\frac{\left|\sum_{i\in\mathcal{D}}\left[r_i^2(r_0,\theta)+d_{\text{v}}^2\right]^{\frac{-m-3}{2}}\right|^2}{\sum_{i\in\mathcal{I}}\left[r_i^2(r_0,\theta)+d_{\text{v}}^2\right]^{-m-3}+Z}, \tag{15}$$

where

$$Z=\frac{N_0\,2W\,\nu}{|\mathcal{F}|}\left[\frac{|C|\,\zeta\,2\pi}{\xi^2\,\eta_{\text{pd}}\,P_{\text{opt}}\,A_{\text{pd}}\,(m+1)\,d_{\text{v}}^{m+1}}\right]^2. \tag{16}$$

Then, the cumulative distribution function (CDF) of the SINR in (15) can be written as

$$F_{\Gamma}(\gamma_{\text{th}}) = \Pr\{\Gamma(r_0,\theta) < \gamma_{\text{th}}\} = \int_{r_0}\int_{\theta} f_{r_0}(r_0)\, f_{\theta}(\theta) \Pr\{\Gamma(r_0,\theta) < \gamma_{\text{th}} | r_0,\theta\}\, \mathrm{d}r_0\, \mathrm{d}\theta, \tag{17}$$

where $f_{r_0}(\cdot)$ and $f_{\theta}(\cdot)$ are the probability density functions (PDFs) that model the user's location in polar coordinates (r_0,θ), and γ_{th} is the SINR threshold value to achieve the target data rate.

In order to estimate the achievable data rate of the VLC system at different locations, we use the well-known Shannon spectral efficiency formula to obtain

$$\text{SE}(r_0,\theta) = \log_2\left[1+\Gamma(r_0,\theta)\right]. \tag{18}$$

Then, assuming that perfect capacity-achieving coding is implemented on the VLC link, the mean data rate that is achievable when the number of subcarriers is large enough (to minimize the effect of granularity when assigning the frequency resources per sector) can be written as

$$\overline{R} \approx \frac{|\mathcal{S}|\, W}{|\mathcal{F}|}\, \text{E}\left\{\log_2\left[1+\Gamma(r_0,\theta)\right]\right\}. \tag{19}$$

C. Illumination requirements to verify for indoor illumination

When designing a VLC system, special attention is needed to meet the illumination regulation for indoor environments. In practice, this implies the verification of two illumination-specific metrics [29]: Firstly, the average illuminance $E_{\text{avg}} = \text{E}\{E_{\text{v}}\}$ [lux] in the whole indoor area must be higher than a given threshold value. Secondly, the illuminance uniformity $U_{\text{light}} = \min\{E_{\text{v}}\}/E_{\text{avg}}$ must be high enough, such that people would not observe notably different lighting levels in the same room. The illuminance at polar coordinates $(r_0,\ \theta)$ can be written as

$$E_{\text{v}}(r_0,\theta) = \Phi \cdot \frac{\sum_i |H_i(r_0,\theta)|}{A_{\text{pd}}}, \tag{20}$$

where $\Phi = K_{\text{e/v}}\, P_{\text{opt}}$ [lm] is the output luminous flux of every AP, A_{pd} is the size of the sensing area of the PD [m^2], and $K_{\text{e/v}}$ [lm/W] is the luminous efficacy of the white light that the LED generates. Note that $K_{\text{e/v}}$ depends on the spectral power density of the aggregate white that the muti-color LEDs generates, as well as on the human eye sensitivity function.

III. Theoretical basis to guarantee SINR homogeneity

The spatial distribution of the SINR in a cellular network is important when designing a wireless communication system. However, the estimation of the SINR that a user would experience at every single location is a hard task, particularly when the network topology is complex. From the whole cellular network point of view, a more practical design approach can be made when the spatial SINR distribution observed in any given *sample* sector is representative for the whole network performance. Therefore, we aim at studying the performance of resource allocation configurations in which the SINR homogeneity requirement is satisfied in the whole multi-cell VLC network (i.e., the spatial SINR distribution is the same regardless of the specific sector). When verifying this requirement, a fair multi-cell network design is achieved and SINR variability for different locations is minimized. As a consequence, the study of the performance in a single sector can be generalized to all the coverage area of the network, without keeping track of the sector/cell indexes. Not complying with the SINR homogeneity requirement does not imply that reliable communication is unfeasible, but rather that the system may not experience the same quality of service in the whole coverage area, as some sectors may have better SINR statistics than others due to varying distances from active serving/interfering APs.

In the remaining of this section we investigate the homogeneity concept in:

(a) **Stand-alone mode (non-cooperative):** In this situation, transmission is made only from the nearest AP. Thus, according to (14), the SINR at polar coordinates (r_0,θ) can be written as

$$\Gamma_{\text{sa}}(r_0,\theta) = \frac{D_0(r_0)}{\sum_{i\in\mathcal{I}} I_i(r_0,\theta)+\sigma^2_{\text{rx}}} = \frac{D(r_0)}{I(r_0,\theta)+\sigma^2_{\text{rx}}}. \tag{21}$$

Since $I(r_0,\theta)$ depends on the azimuth angle θ, the SINR homogeneity in the whole VLC network is attainable only if $I(r_0,\theta)$ maintains the same spatial distribution at every sector.

(b) **Cooperation mode:** In this case, cooperation among neighboring APs is implemented and, according to (14), the SINR at user location (r_0,θ) attains the form

$$\Gamma_{\text{coop}}(r_0,\theta) = \frac{\sum_{i\in\mathcal{D}} D_i(r_0,\theta)}{\sum_{i\in\mathcal{I}} I_i(r_0,\theta)+\sigma^2_{\text{rx}}} = \frac{D(r_0,\theta)}{I(r_0,\theta)+\sigma^2_{\text{rx}}}. \tag{22}$$

Note that besides the *stand-alone mode* conditions that the term $I(r_0,\theta)$ in the denominators of (21) and (22) should verify, new conditions must also be fulfilled in the numerator $D(r_0,\theta)$ of (22) to guarantee the SINR homogeneity in the *cooperation mode*.

A. Stand-alone mode (no cooperation among adjacent cells)

The following statements should be verified *at different levels* to guarantee the SINR homogeneity *without cooperation* in the whole coverage area of the VLC network:

Statement 1: (Tessellation level) The cell cluster size must be a rhombic number, verifying $Q_0 \in \left\{i^2+j^2+ij\right\}\ \forall\, i,j \in \mathbb{N}$. Any cellular network can increase its aggregate data rate by re-using communication resources in the different cells. In practice, this gain depends on resource-reuse factor, which is defined as the rate at which a certain resource is allocated throughout the cells of the network. For hexagonal cells, the cluster size controls the reuse distance $R_{\text{d}} = \widetilde{R}\sqrt{3Q_0}$. However, to have a tessellation with hexagonal cells that complies with the same reuse distance with six equidistant cells, the cluster size must verify $Q_0 \in \left\{i^2+j^2+ij\right\}\ \forall\, i,j \in \mathbb{N}$.

Proof: The analogy between an RF cellular system and the proposed VLC multi-cell network applies straightforwardly. The LED horizontal radiation pattern is similar to the one provided by an omnidirectional RF antenna, and

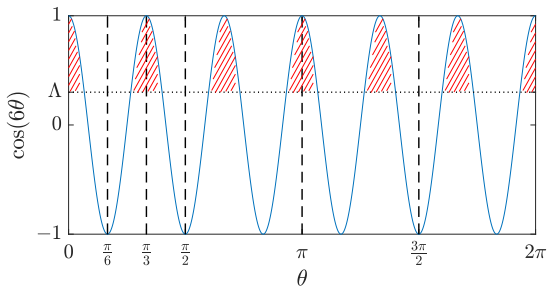

Fig. 4: Illustration of the probability (red shaded area) that function $\cos(6\theta)$ takes values larger than Λ for different θ.

resources in the VLC network (i.e. combinations of chip colors and electrical frequency sub-bands) are analogous to time slots/frequency bands/spreading codes in RF cellular systems. Therefore, it is well-known that a tessellation with hexagonal cells is correctly designed if $Q_0 \in \{i^2 + j^2 + ij\}\ \forall\, i,j \in \mathbb{N}$, as demonstrated in [30]. ■

Statement 2: (Cell level) A VLC cell can only be divided into $|\mathcal{S}| \in \{1,2,3,4,6,12\}$ *sectors*. Here, we identify the number of sectors in which a cell can be divided in order to verify the SINR homogeneity in each sector. Assuming that *Statement 1* is satisfied, the interfering APs are equidistant, with angular separation of $\pi/3$. Then, the interference power coming from the APs follows a flower model with respect to θ, which can be approximated as follows [22] [31]:

$$I(r_0,\theta) \approx \frac{I_{\frac{\pi}{6}}(r_0) + I_0(r_0)}{2} + \frac{\left|I_{\frac{\pi}{6}}(r_0) - I_0(r_0)\right|}{2}\cos(6\theta), \quad (23)$$

where $I_{\frac{\pi}{6}}(r_0)$ and $I_0(r_0)$ are the interference power at radial coordinate r_0 and angular coordinate $\theta = \frac{\pi}{6}$ rad and $\theta = 0$ rad, respectively. The CDF for the SINR conditioned to r_0 can be determined by combining (23) with (21), i.e.,

$$P\left[\Gamma_{\text{sa}}<\gamma_{\text{th}}|r_0\right] = P\left[\cos(6\theta) > \left\{\frac{2D(r_0)\frac{1}{\gamma_{\text{th}}} - \left[I_{\frac{\pi}{6}}(r_0)+I_0(r_0)\right] - 2\sigma^2_{\text{rx}}}{\left|I_{\frac{\pi}{6}}(r_0) - I_0(r_0)\right|}\right\}\middle| r_0\right]$$
$$= P[\cos(6\theta)>\Lambda|r_0]. \quad (24)$$

The function $\cos(6\theta)$ has period $p = \frac{\pi}{3}$ rad, as shown in Fig. 4. Then, $P[\cos(6\theta) > \Lambda|r_0]$ for $\theta \in [0,2\pi)$ is equivalent to $P[\cos(6\theta) > \Lambda|r_0]$ for $\theta \in \left[0, \frac{pk}{2}\right)$ with $k \in \mathbb{N}$, where k is the possible number of semi-periods in Fig. 4. Since we aim to divide a cell in sectors, $\frac{pk}{2}\cdot|\mathcal{S}| = \frac{\pi k}{6}\cdot|\mathcal{S}| = 2\pi$ must be verified, where $|\mathcal{S}| \in \mathbb{N}$ is the number of sectors in which a cell is divided, as defined in Table I. Then, the different possibilities are $k = 1$ ($|\mathcal{S}| = 12$), $k = 2$ ($|\mathcal{S}| = 6$), $k = 3$ ($|\mathcal{S}| = 4$), $k = 4$ ($|\mathcal{S}| = 3$), $k = 6$ ($|\mathcal{S}| = 2$), and $k = 12$ ($|\mathcal{S}| = 1$). To sum up, only the number of sectors $|\mathcal{S}| \in \{1,2,3,4,6,12\}$ are possible to guarantee the SINR homogeneity at the *cell level*.

Proof: This statement determines that $P\left[\Gamma_{\text{sa}}<\gamma_{\text{th}}|r_0\right] = P[\cos(6\theta)>\Lambda|r_0] = P[\cos(\omega)>\Lambda|r_0]$ is the same regardless of the sector. Let us assume that $k_{\text{high}} = \left\lceil \frac{\omega_{\max}}{2\pi} \right\rceil$ and $k_{\text{low}} = \left\lfloor \frac{\omega_{\max}}{2\pi} \right\rfloor$ represent the number of semi-loops in the intervals $[0,\pi)$ and $[\pi,2\pi)$ that ω spins, respectively, where $\omega_{\max} = \max\{\omega\}$. Then, considering all possible sectorization modes, i.e.,

- $|\mathcal{S}| = 1 \Rightarrow \theta \in [0,2\pi] \Rightarrow \omega \in [0,12\pi] \Rightarrow k_{\text{high}} = 6, k_{\text{low}} = 6, f_\omega(\omega) = \frac{1}{12\pi}$,
- $|\mathcal{S}| = 2 \Rightarrow \theta \in [0,\pi] \Rightarrow \omega \in [0,6\pi] \Rightarrow k_{\text{high}} = 3, k_{\text{low}} = 3, f_\omega(\omega) = \frac{1}{6\pi}$,
- $|\mathcal{S}| = 3 \Rightarrow \theta \in [0,\frac{2\pi}{3}] \Rightarrow \omega \in [0,4\pi] \Rightarrow k_{\text{high}} = 2, k_{\text{low}} = 2, f_\omega(\omega) = \frac{1}{4\pi}$,
- $|\mathcal{S}| = 4 \Rightarrow \theta \in [0,\frac{\pi}{2}] \Rightarrow \omega \in [0,3\pi] \Rightarrow k_{\text{high}} = 2, k_{\text{low}} = 1, f_\omega(\omega) = \frac{1}{3\pi}$,
- $|\mathcal{S}| = 6 \Rightarrow \theta \in [0,\frac{\pi}{3}] \Rightarrow \omega \in [0,2\pi] \Rightarrow k_{\text{high}} = 1, k_{\text{low}} = 1, f_\omega(\omega) = \frac{1}{2\pi}$,
- $|\mathcal{S}| = 12 \Rightarrow \theta \in [0,\frac{\pi}{6}] \Rightarrow \omega \in [0,\pi] \Rightarrow k_{\text{high}} = 1, k_{\text{low}} = 0, f_\omega(\omega) = \frac{1}{\pi}$,

where $f_\omega(\omega)$ is the PDF for ω for each case. Thus, $P\left[\Gamma_{\text{sa}} < \gamma_{\text{th}}|r_0\right] = P[\cos(\omega)>\Lambda|r_0] = \sum_{k=1}^{k_{\text{high}}} \int_{2\pi(k-1)}^{2\pi(k-1)+\arccos(\Lambda)} f_\omega(\omega)\mathrm{d}\omega + \sum_{k=1}^{k_{\text{low}}} \int_{2\pi k-\arccos(\Lambda)}^{2\pi k} f_\omega(\omega)\mathrm{d}\omega = \frac{\arccos(\Lambda)}{\pi}, \ \forall\left(k_{\text{high}}, k_{\text{low}}\right)$. ■

Statement 3: (Sector level) The orientation that a sector takes in the tessellation is irrelevant to verify the SINR homogeneity requirement, except for $|\mathcal{S}| \in \{4,12\}$. This statement identifies the way in which the number of sectors per cell identified in *Statement 2* must be oriented:

- If $|\mathcal{S}| \in \{1,2,3,6\}$: The orientation of the applied sectorization in each cell is irrelevant; thus, the study of a sector can always be generalized to the whole cell and tessellation.
- If $|\mathcal{S}| \in \{4,12\}$: The sector must be delimited by the following angles:
  - For $|\mathcal{S}| = 4$: $b\pi/6 \le \theta_{\text{sector}} \le (b+3)\pi/6, \quad 0 \le b \le 9$,
  - For $|\mathcal{S}| = 12$: $b\pi/6 \le \theta_{\text{sector}} \le (b+1)\pi/6, \quad 0 \le b \le 11$,

where b is the starting angular point of the sectorization, while the rest of the sectors must be delimited by consecutive angles. Angle directions considered in this paper are shown in Fig. 2a.

Proof: Because of the periodicity of the function $\cos(6\theta)$, the calculation of $P[\cos(\omega) > \Lambda]$ in a sector does not depend on the sector position if the number of semi-loops $[0,\pi)$ and $[\pi,2\pi)$ are integer, verifying $k_{\text{high}} = k_{\text{low}} = \frac{\omega_{\max}}{2\pi} \in \mathbb{N}$. Note that in our case:

- $\frac{\omega_{\max}}{2\pi} \in \mathbb{N} \iff |\mathcal{S}| \in \{1,2,3,6\}$.
- $\frac{\omega_{\max}}{2\pi} \notin \mathbb{N} \iff |\mathcal{S}| \in \{4,12\}$. In this case, the number of semi-loops $[0,\pi)$ and $[\pi,2\pi)$ that ω takes are not the same; due to that, sectors must be limited by the following angles:
  - For $|\mathcal{S}| = 4$: $bp/2 \le \theta_{\text{sector}} \le (b+3)p/2, \quad 0 \le b \le 9$,
  - For $|\mathcal{S}| = 12$: $bp/2 \le \theta_{\text{sector}} \le (b+1)p/2, \quad 0 \le b \le 11$,

  where $p = \frac{\pi}{3}$ is the period of $\cos(6\theta)$. As shown in Fig. 4, when $|\mathcal{S}| = 4, 12$, $P\left[\cos(6\theta) > \Lambda\right]$ is not equal when the requirements are not satisfied because the section area varies.

■

B. Cooperation mode (with cooperation among adjacent cells)

When cooperation among APs is implemented, spatial SINR homogeneity may be lost even when the homogeneity *without*

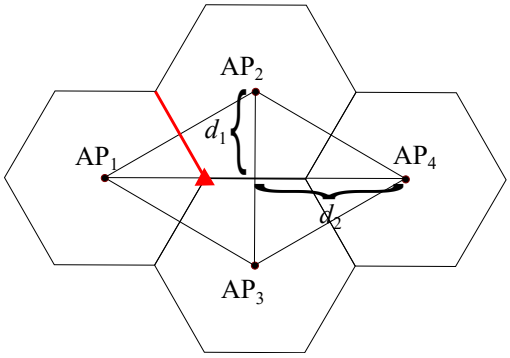

Fig. 5: A cooperative set with four APs cannot provide a homogeneous distribution of the SINR with cooperation, as no point is equidistant to all the APs. Red line: Set of equidistant points between two APs (AP_1 and AP_2). Red solid triangle: Unique equidistant point between three APs (AP_1, AP_2 and AP_3).

TABLE II: Minimum number of resources for cooperation mode configurations with SINR homogeneity requirement.

$\lvert\mathcal{S}\rvert$	$M = S_{\text{coop}}$	Q_{coop}	$N_{\min} = S_{\text{coop}} \cdot Q_{\text{coop}}$
1	1	1(=$\lvert\mathcal{S}\rvert$)	1
1	2	1	2
1	3	1	3
2	1	2(=$\lvert\mathcal{S}\rvert$)	2
2	2	2	4
2	3	2	6
3	1	3(=$\lvert\mathcal{S}\rvert$)	3
3	2	3	6
3	3	3	9
4	1	4(=$\lvert\mathcal{S}\rvert$)	4
4	2	4	8
6	1	6(=$\lvert\mathcal{S}\rvert$)	6
6	2	6	12
6	3	6	18
12	1	12(=$\lvert\mathcal{S}\rvert$)	12
12	2	12	24
12	3	12	36

cooperation is observed. Thus, additional statements must be identified to maintain the SINR homogeneity feature when multi-point transmission is used.

Statement 4: (Resource distribution level) In cooperation mode, $N = |C| \cdot |\mathcal{F}| \geq S_{\text{coop}} \cdot Q_{\text{coop}}$ *must be satisfied.* The maximum number of available resources in any cooperation transmission configuration must verify $N = |C| \cdot |\mathcal{F}| \geq S_{\text{coop}} \cdot Q_{\text{coop}}$, where S_{coop} is the number of sectors in the cooperation area and Q_{coop} is the number of cooperation areas in which every AP cooperates.

Proof: If $N < S_{\text{coop}} \cdot Q_{\text{coop}}$, then at least one AP in the cooperation set would have to transmit information to more sectors than the number of available orthogonal resources. This is not possible, since the information transmitted by the same AP to users on different sectors should be done on orthogonal resources (i.e., different frequency sub-bands per LED color). ■

Statement 5: (Cooperation set level) The inequality $1 \leq \mu \cdot M = S_{\text{coop}} \leq 3$ *must be verified for a correct cooperation mode configuration, where* $\mu = 1, 2, \ldots$ *represents the number of sectors per AP of the cooperation set.* The sectors where the APs cooperate (S_{coop}) must be a multiple of the number

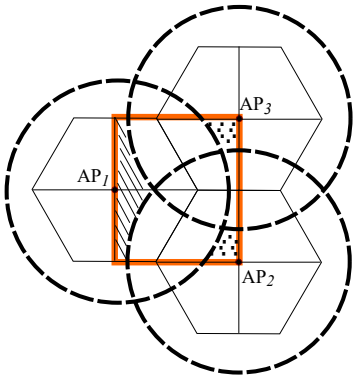

(a) Resource allocation configuration with $|\mathcal{S}| = 4$, $M = 3$, and $S_{\text{coop}} = 4$ (SINR homogeneity is not verified).

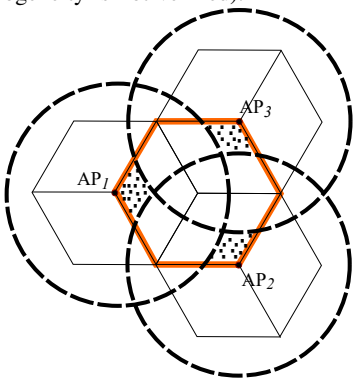

(b) Resource allocation configuration with $|\mathcal{S}| = 3$, $M = 3$, and $S_{\text{coop}} = 3$ (SINR homogeneity is verified).

Fig. 6: Demonstration of the fact that M must be equal to S_{coop} for SINR homogeneity in cooperation mode.

of cooperating APs (M). Besides, as the deployment of APs is done to establish a hexagonal tessellation of cells, the number of cooperating APs cannot be larger than 3 to prevent imbalances in the received signal power (i.e., numerator of SINR formula).

Proof: In order to get the same CDF for the SINR of each sector in cooperation mode, the center of the cooperative set must be equidistant to each of the cooperating APs. In the union area of four APs, there is no point that is equidistant to all of them, as shown in Fig. 5. In contrast, the red line and the solid triangle represent the equidistant points between two and among three APs, respectively. Therefore, it is not possible to create a cooperation set of size $M > 3$ that maintains a homogeneous spatial SINR distribution among sectors. Besides, $\mu \cdot M = S_{\text{coop}}$ with $\mu = 1, 2, \ldots$ is a necessary condition to verify SINR homogeneity, since the union of coverage areas of the cooperating APs must be equal at each sector in which they cooperate. Fig. 6a shows a sample cooperative mode configuration with $|\mathcal{S}| = 4$, $M = 3$ and $S_{\text{coop}} = 4$, in which the requirement $\mu \cdot M = S_{\text{coop}}$ is *not* verified. Note that the coverage areas of APs, represented by dashed circles, are not equal at each sector where they cooperate (i.e., the areas represented by parallel lines and by points are not equal). In contrast, Fig. 6b illustrates the case

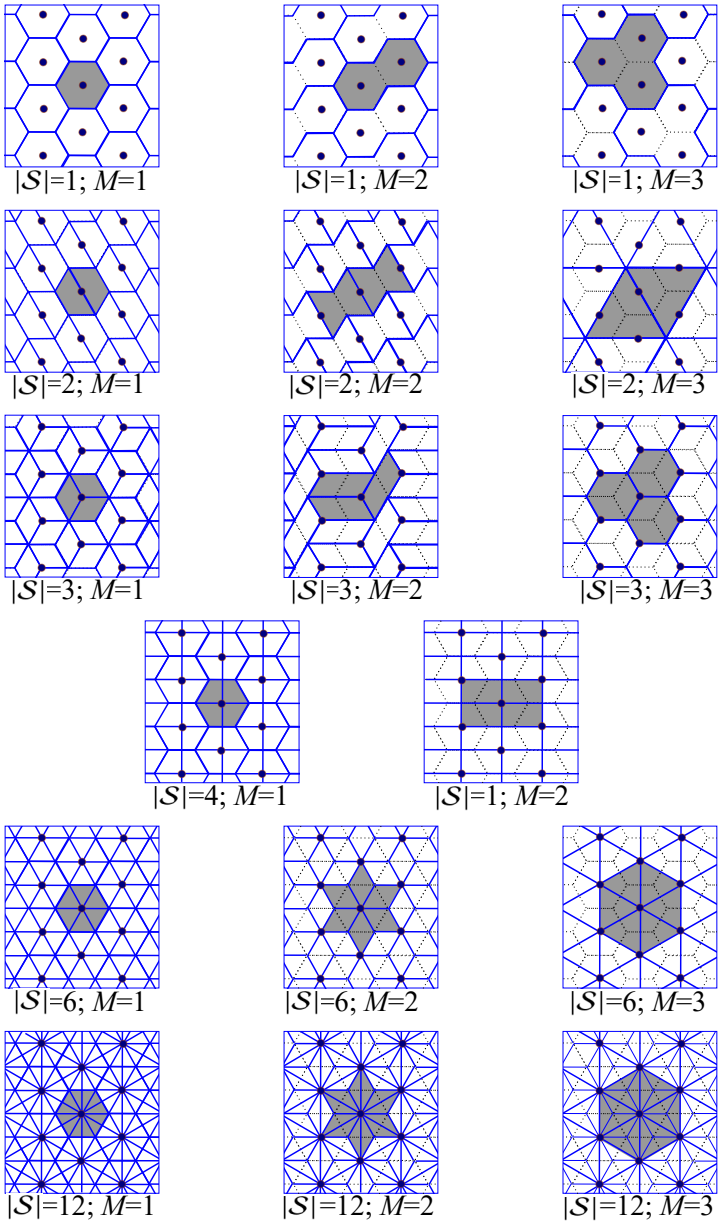

Fig. 7: Illustration of the cooperation sets that can be established for different number of sectors per cell. Solid dots represent APs, blue lines identify sector boundaries, and shaded areas mark the sectors served by the central AP.

where $M = S_{\text{coop}} = 3$ ($\mu = 1$), and shows that the SINR homogeneity at each sector is verified. ■

Table II summarizes the parameters of the cooperation mode configurations that verify *Statement* 4 and *Statement* 5 simultaneously, including the minimum number of orthogonal resources needed to implement each of them. For clarification purposes, the table also includes the configurations when no cooperation is performed ($M = 1$), in which case $Q_{\text{coop}} = |\mathcal{S}|$. Note that the setup with $|\mathcal{S}| = 4$ and $M = 3$ is not included because $S_{\text{coop}} \neq M$, as shown in Fig. 6.

Statement 6: (Final cluster level) The final cluster size in a cooperation mode setup that verifies SINR homogeneity is given by $Q = Q_0 \; \forall \; \{|\mathcal{S}|, M\} \backslash \{|\mathcal{S}| = 2, M = 3\} \cup \{|\mathcal{S}| = 3, M = 2\}$. *In the latter two cases,* $Q = \text{LCM}(Q_0, M)$. The final cluster *with* cooperation (Q) is the same as the initial cluster *without* cooperation (Q_0), except for the cooperation setups with more than one sectorization mode. In these two cases, which are configurations $\{|\mathcal{S}| = 2, M = 3\}$ and $\{|\mathcal{S}| = 3, M = 2\}$, Q is the least common multiple (LCM) of Q_0 and M, where M denotes the number of cooperating APs (that equals the number of sectorization modes in both cases).

Proof: The cooperation sets presented in Table II are visualized in Fig. 7. The shaded regions are the areas where the central AP serves its associated users, and cooperates with the neighboring APs when $M \geq 2$. Note that the sectorization for every cell *without* cooperation ($M = 1$) is the same as the sectorization for every cell *with* cooperation ($M \geq 2$), except for the configurations with $\{|\mathcal{S}| = 2, M = 3\}$ and $\{|\mathcal{S}| = 3, M = 2\}$. In these two cases, cells must be sectorized in three and two sectorization orientations, respectively, increasing the

TABLE III: Cluster sizes (numbers with no brackets) and possible cooperation setups (numbers between brackets) for a RGB LED ($|C| = 3$). Blue-shaded values are for configurations verifying all statements for SINR homogeneity.

$\lvert\mathcal{F}\rvert$	Freq. bands (per color)	1	2	3	4	5	6	7	8	9
N ($\lvert\mathcal{F}\rvert\cdot\lvert C\rvert$)	Orthogonal resources	3	6	9	12	15	18	21	24	27
# sectors	$\lvert\mathcal{S}\rvert = 1$	$3_{(M=1,2,3)}$	6	$9_{(M=1,2,3)}$	$12_{(M=1,2,3)}$	15	18	$21_{(M=1,2,3)}$	24	$27_{(M=1,2,3)}$
	$\lvert\mathcal{S}\rvert = 2$	1.5	$3_{(M=1,2,3)}$	4.5	6	7.5	$9_{(M=1,2,3)}$	10.5	$12_{(M=1,2,3)}$	13.5
	$\lvert\mathcal{S}\rvert = 3$	$1_{(M=1)}$	2	$3_{(M=1,3)}$	$4_{(M=1,2,3)}$	5	6	$7_{(M=1,3)}$	8	$9_{(M=1,3)}$
	$\lvert\mathcal{S}\rvert = 4$	0.75	1.5	2.25	$3_{(M=1,2)}$	3.75	4.5	5.25	6	6.75
	$\lvert\mathcal{S}\rvert = 6$	0.5	$1_{(M=1)}$	1.5	2	2.5	$3_{(M=1,2,3)}$	3.5	$4_{(M=1,2,3)}$	4.5
	$\lvert\mathcal{S}\rvert = 12$	0.25	0.5	0.75	$1_{(M=1)}$	1.25	1.5	1.75	2	2.25

TABLE IV: Cluster sizes (numbers with no brackets) and possible cooperation setups (numbers between brackets) for a RGBY LED ($|C| = 4$). Blue-shaded values are configurations verifying all statements for SINR homogeneity.

$\lvert\mathcal{F}\rvert$	Freq. bands (per color)	1	2	3	4	5	6	7	8	9
N ($\lvert\mathcal{F}\rvert\cdot\lvert C\rvert$)	Orthogonal resources	4	8	12	16	20	24	28	32	36
# sectors	$\lvert\mathcal{S}\rvert = 1$	$4_{(M=1,2,3)}$	8	$12_{(M=1,2,3)}$	$16_{(M=1,2,3)}$	20	24	$28_{(M=1,2,3)}$	32	$36_{(M=1,2,3)}$
	$\lvert\mathcal{S}\rvert = 2$	2	$4_{(M=1,2)}$// $12_{(M=3)}$	6	8	10	$12_{(M=1,2,3)}$	14	$16_{(M=1,2)}$// $48_{(M=3)}$	18
	$\lvert\mathcal{S}\rvert = 3$	1.33	2.67	$4_{(M=1,2,3)}$	5.33	6.67	8	9.33	10.67	$12_{(M=1,2,3)}$
	$\lvert\mathcal{S}\rvert = 4$	$1_{(M=1)}$	2	3	$4_{(M=1,2)}$	5	6	$7_{(M=1,2)}$	8	$9_{(M=1,2)}$
	$\lvert\mathcal{S}\rvert = 6$	0.67	1.33	2	2.67	2.33	$4_{(M=1,2,3)}$	4.67	5.33	6
	$\lvert\mathcal{S}\rvert = 12$	0.33	0.67	$1_{(M=1)}$	1.33	1.67	2	2.33	2.67	$3_{(M=1,2,3)}$

reuse factor as $Q = \text{LCM}(Q_0, 3)$ for $\{|\mathcal{S}| = 2, M = 3\}$ and $Q = \text{LCM}(Q_0, 2)$ for $\{|\mathcal{S}| = 3, M = 2\}$. ■

Finally, for the sake of clarification, the shaded cells in Table III (RGB LED) and Table IV (RGBY LED) represent the configurations in terms of the number of frequency sub-bands per color ($|\mathcal{F}|$) and the number of sectors per cell ($|\mathcal{S}|$) that comply with *Statements* 1-6, verifying an homogeneous spatial SINR distribution on the whole tessellation. Numbers without brackets indicate the cluster size Q, whereas numbers between brackets show the number of possible cooperating APs (M). In the remainder of this paper, only the *shaded* configurations are studied.

IV. Simulation Results and Performance Analysis

After identifying the resource allocation configurations that provide SINR homogeneity, we are now ready to study their performance for different network planning parameters, such as the cell radius and LED half-power semi-angle. Note that the verification of illumination requirements depends on the layout of the VLC network, but not on the resource allocation that is performed.

Numerical simulations are performed in a three-tier multi-cell layout, configuring the VLC network and links according to the parameters reported in Table V. The flat-response bandwidth for the different LED chips is selected to be 25 MHz, a value that is aligned with the ones observed in commercial multi-color LEDs. The DCO-OFDM scheme that is utilized in this paper assumes 512 subcarriers that occupy the whole electrical modulation bandwidth in each LED color. To make fair comparisons between study cases with different cell radius R, the optical transmit power per unit area $P_{\text{opt/Area}}$ is fixed to 2 W/m^2, a value that is consistent with the optical transmit power (P_{opt}) used in other references [7]. Thus, it is possible to see that $P_{\text{opt}} = P_{\text{opt/Area}} \cdot \pi R^2$, and that this power varies between 2.26 and 56.55 W when the cell radius grows from $R_{\text{min}} = 0.6$ to $R_{\text{max}} = 3.0$ m. Also, the impact of optical filters placed in front of the PDs is neglected, as they do not affect the homogeneity definition because the proposed cooperative mode configurations divide the service area in sectors with identical characteristics.

TABLE V: Simulation parameters of the VLC system, including VLC network layout and VLC link configuration.

Parameter	Description	Value	Unit
R	Circular cell radius	0.6–3	[m]
d_{v}	Vertical distance between AP and PD	2.25	[m]
$\phi_{1/2}$	Half-power semi-angle of the LED	25–75	[deg.]
$P_{\text{opt/Area}}$	Optical transmit power per unit area	2	[W/m^2]
$K_{\text{e/v}}$	Luminous efficacy of generated white light	300	[lm/W]
W	Bandwidth of LED chip	25	[MHz]
ζ	Ratio DC-standard deviation (DCO-OFDM)	5.05	[dB]
η_{pd}	APD responsivity	16	[A/W]
A_{pd}	APD physical area	3.14	[mm^2]
K	Number of subcarriers (IFFT size)	512	
$E_{\text{v,ab}}$	Illuminance from ambient light	100	[lux]
T_{abs}	Absolute temperature	300	[K]
R_{L}	Receiver load resistance	500	[Ω]

A. Verification of the illumination requirements

Fig. 8 shows the average illuminance E_{avg} and illuminance uniformity U_{light} that the VLC system provides for different R and $\phi_{1/2}$. As expected, the *most uniform* illumination (i.e., highest U_{light}) is observed when using the *least directional* LEDs (i.e., highest $\phi_{1/2}$), as the emitted light is distributed

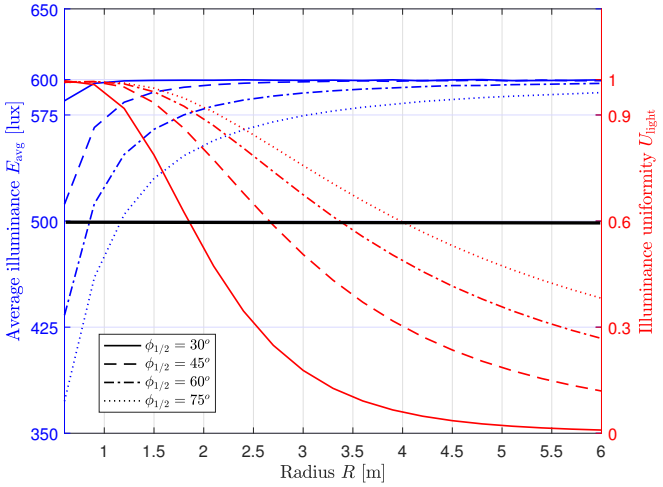

Fig. 8: Average illuminance E_{avg} (blue lines) and illuminance uniformity U_{light} (red lines) as function of the circular cell radius R for different half-power semi-angle $\phi_{1/2}$. Note that illumination metrics only depend on the VLC network layout (not on the communication mode or resource allocation configuration that is utilized).

most homogeneously. The opposite situation takes place when using LEDs with high directivity (i.e., low $\phi_{1/2}$), as in this case the emitted light is concentrated on spots around the cell centers, where the incidence angle is small. Thus, larger E_{avg} values are achieved with most directional LEDs, but these illumination levels are least homogeneously distributed. The maximum average illuminance is achieved when R grows large, and is given by

$$\lim_{R\to\infty} \mathrm{E}\left\{ \frac{\Phi \sum_i |H_i(r_0,\theta)|}{A_{\text{pd}}} \right\} = \lim_{R\to\infty} \int_0^R \frac{\Phi\, |H_0(r_0)|}{A_{\text{pd}}} f_{r_0}(r_0)\, \mathrm{d}r_0$$

$$= \lim_{R\to\infty} P_{\text{opt/Area}}\, K_{\text{e/v}}\, (m+1)\, h^{m+1} \int_0^R \frac{r_0}{\left(r_0^2 + h^2\right)^{\frac{m+3}{2}}}\, \mathrm{d}r_0$$

$$= P_{\text{opt/Area}}\, K_{\text{e/v}}. \tag{25}$$

Note that $\lim_{R\to\infty} \sum_i |H_i(r_0,\theta)| = |H_0(r_0)|$ because adjacent APs are far away and, if the received power comes only from the nearest AP (i.e., the AP with index '0' in the center of the three-tier simulation scenario that was proposed), aggregate channel H in this situation becomes mainly dependent on the *large value* that the horizontal distance r_0 takes. Besides, it is assumed that users are uniformly distributed on the area of the circular cell and, thus, $f_{r_0}(r_0) = \frac{2\, r_0}{R^2}$. Since the optical power per unit area is fixed, the output luminous flux is given by $\Phi = P_{\text{opt/Area}}\, \pi\, R^2\, K_{\text{e/v}}$.

For typical office scenario in which writing, typing or reading tasks are carried out, illumination conditions $E_{\text{avg}} > 500$ lux and $U_{\text{light}} > 0.6$ must be verified [29]. Thus, those VLC network settings (i.e., R and $\phi_{1/2}$) that satisfy both illumination requirements are valid to be used in actual indoor scenarios. Note that the working points that appear above the horizontal black line in Fig. 8 verify both mean illumination and illumination uniformity requirements.

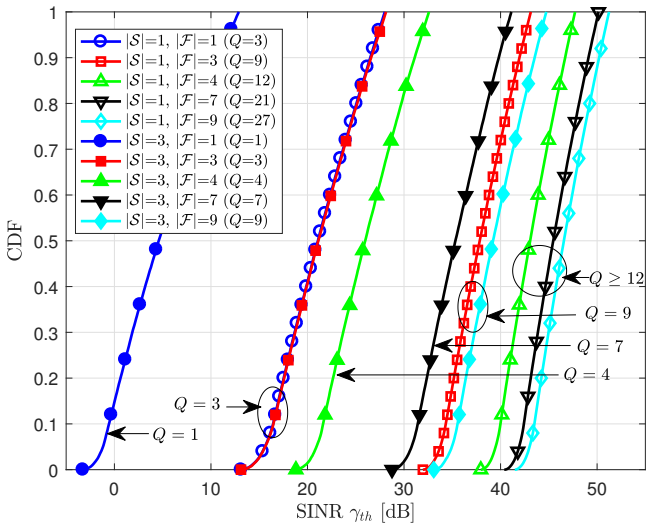

(a) RGB LEDs ($|C| = 3$).

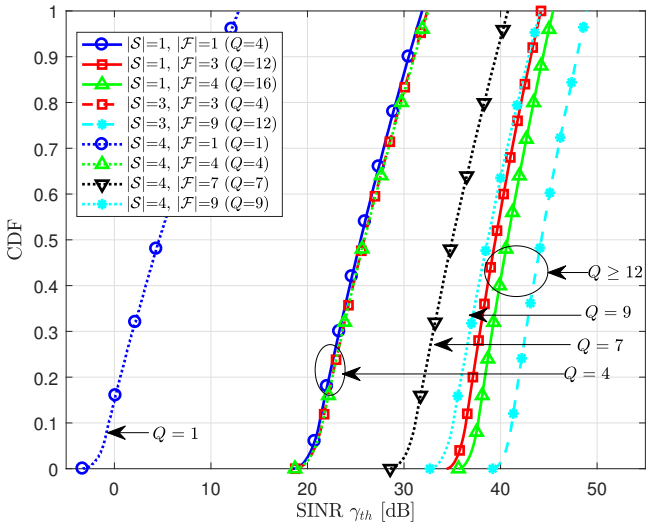

(b) RGBY LEDs ($|C| = 4$).

Fig. 9: Cumulative distribution function for the SINR of different resource allocation configurations in stand-alone/no-cooperation transmission mode ($M = 1$). VLC network layout parameters: $R = 1.5$ m and $\phi_{1/2} = 60°$.

B. Performance of resource allocation configurations with stand-alone transmission ($M = 1$)

The CDF for the SINR that corresponds to the different resource allocation configurations in case of stand-alone transmission mode ($M = 1$) with RGB and RGBY LEDs are presented in Fig. 9a and Fig. 9b, respectively. As expected, the SINR improves when the cluster size Q grows. For low Q, the (optical) interference power is stronger than the noise power; therefore, all resource allocation configurations with same cluster size Q experience the same SINR performance. Note that this effect is observed in configurations $\{|C|{=}3, |\mathcal{S}|{=}1, M{=}1, |\mathcal{F}|{=}1\}$ and $\{|C|{=}3, |\mathcal{S}|{=}3, M{=}1, |\mathcal{F}|{=}3\}$ for $Q{=}3$, and $\{|C|{=}4, |\mathcal{S}|{=}1, M{=}1, |\mathcal{F}|{=}1\}$, $\{|C|{=}4, |\mathcal{S}|{=}3, M{=}1, |\mathcal{F}|{=}3\}$ and $\{|C|{=}4, |\mathcal{S}|{=}4, M{=}1, |\mathcal{F}|{=}4\}$ for $Q{=}4$. In contrast,

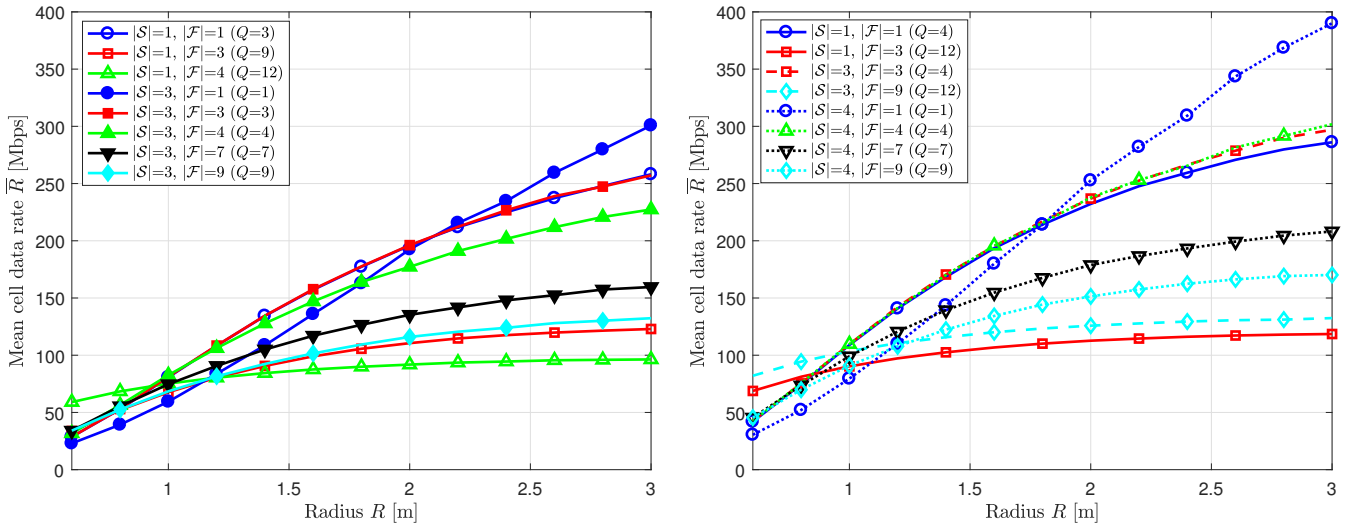

(a) RGB LEDs ($|C|$ = 3). (b) RGBY LEDs ($|C|$ = 4).

Fig. 10: Mean cell data rate $\overline{R}$ as function of the circular radius R of the VLC cells when $\phi_{1/2} = 60°$ and different resource allocation configurations are utilized in stand-alone transmission mode ($M = 1$).

in those resource allocation configurations in which Q is large, the effect of the noise power gains importance and, due to that, the specific values that ν, $|C|$ and $|\mathcal{F}|$ take become relevant when computing the SINR in reception using (15)-(16). Thus, when comparing two resource allocation configurations with equally large $Q_1 = \frac{|C_1||\mathcal{F}_1|}{|\mathcal{S}_1|}$ and $Q_2 = \frac{|C_2||\mathcal{F}_2|}{|\mathcal{S}_2|}$, the SINR gap is in the order of $\frac{|\mathcal{F}_1|\nu_2|C_2|^2}{|\mathcal{F}_2|\nu_1|C_1|^2}$. As an example, when comparing the resource allocation configurations with $\{|C|$=3, $|\mathcal{S}|$=1, M=1, $|\mathcal{F}|$=4$\}$ and $\{|C|$=4, $|\mathcal{S}|$=3, M=1, $|\mathcal{F}|$=9$\}$, both of them with $Q = 12$ and $\nu_1 = \nu_2 = 1$, the SINR gap that results is in the order of $10\log_{10}(\frac{4\times16}{9\times9}) \approx -1$ dB. In addition, we note that for noise-limited situations (i.e. large Q), those resource allocation configurations with large $|\mathcal{F}|$ perform better since the noise power in reception is reduced by the same factor $|\mathcal{F}|$ after frequency-domain demultiplexing, as indicated in (16). For example, the resource allocation configuration with $\{|C|$=4, $|\mathcal{S}|$=3, M=1, $|\mathcal{F}|$=9$\}$ offers a better SINR performance than $\{|C|$=4, $|\mathcal{S}|$=1, M=1, $|\mathcal{F}|$=4$\}$, even when the second configuration has a larger Q. Finally, when stand-alone transmission configurations with RGB and RGBY LEDs are compared, no notable SINR differences are observed when comparing resource allocation configurations with same cluster size Q.

The mean cell data rate formulated in (19) is shown in Fig. 10a and Fig. 10b when using RGB and RGBY LEDs, respectively. For the sake of clarity, only $\{|C|$=3, $|\mathcal{S}|$=1$\}$ and $\{|C|$=3, $|\mathcal{S}|$=3$\}$ configurations are included in Fig. 10a, and $\{|C|$=4, $|\mathcal{S}|$=1$\}$, $\{|C|$=4, $|\mathcal{S}|$=3$\}$ and $\{|C|$=4, $|\mathcal{S}|$=4$\}$ in Fig. 10b. As expected, the larger is the radius of the cell, the higher is the mean data rate that is achievable since the inter-cell interference power that is presented in the VLC network is reduced. When the interference power becomes lower than the noise power (large R values), resource allocation configurations that result in small cluster sizes Q give the best performance. However, as R decreases, larger Q values are needed to keep the inter-cell interference power under control. For example, when using RGB LEDs in small cell scenarios with $R < 0.9$ [m], resource allocation configurations with $Q = 12$ offer the highest mean cell data rate performance, whereas configurations with $Q = 4$ ($Q = 3$) behave better when the cell radius lies in the $0.9 < R < 1.1$ ($1.1 < R < 2$) [m] range. For cell radius $R > 2$ [m], resource allocation configurations with $Q = 1$ are the best choice. We note that the same phenomenon takes place when RGBY LEDs are used. Finally, for large R cases in which effect of noise power gains relevance, minor performance differences are observed when comparing configurations with the same Q (e.g., resource allocation schemes with $Q = 9$ in RGB LEDs and with $Q = 4$ in RGBY LEDs).

Note that when comparing Fig. 10a with Fig. 10b, and in line with the theoretical analysis that can be done in (19), it is possible to see that resource allocation configurations with RGBY LEDs provide cell data rate gains in the order of 33% with respect to an equivalent configuration with RGB LEDs (i.e., same cluster size Q). This is because the SINR is similar in both RGB and RGBY LED configurations dominated by optical interference, but in the RGBY LED case there are 4/3 times more electrical bandwidth available when compared to its RGB LED counterpart.

The effect that the half-power semi-angle $\phi_{1/2}$ has on the mean cell data rate $\overline{R}$ of different resource allocation configurations is represented in Fig. 11a and Fig. 11b when using RGB and RGBY LEDs, respectively. As expected, the mean cell data rate performance degrades notably as $\phi_{1/2}$ increases, because a larger inter-cell interference power is generated when irradiating wider spatial light-beams. Therefore, those resource allocation configurations that are most affected by strong inter-cell interference (low Q values) experience a

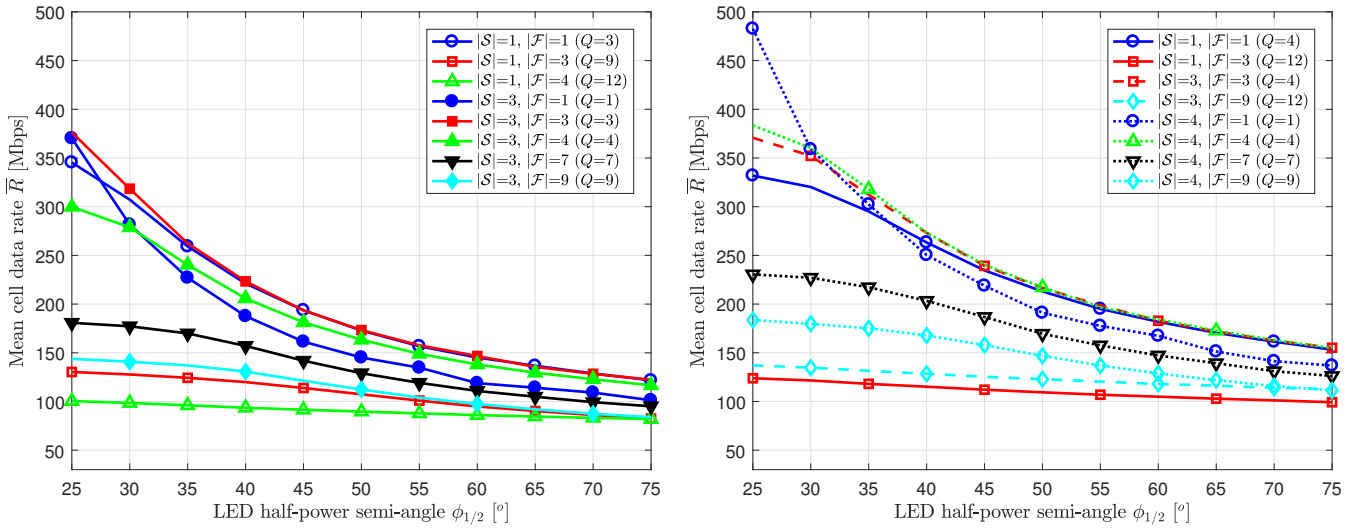

(a) RGB LEDs ($|C|$ = 3). (b) RGBY LEDs ($|C|$ = 4).

Fig. 11: Mean cell data rate $\overline{R}$ as function of the LED half-power semi-angle $\phi_{1/2}$ when $R = 1.5$ m and different resource allocation configurations are utilized in stand-alone transmission mode (M = 1).

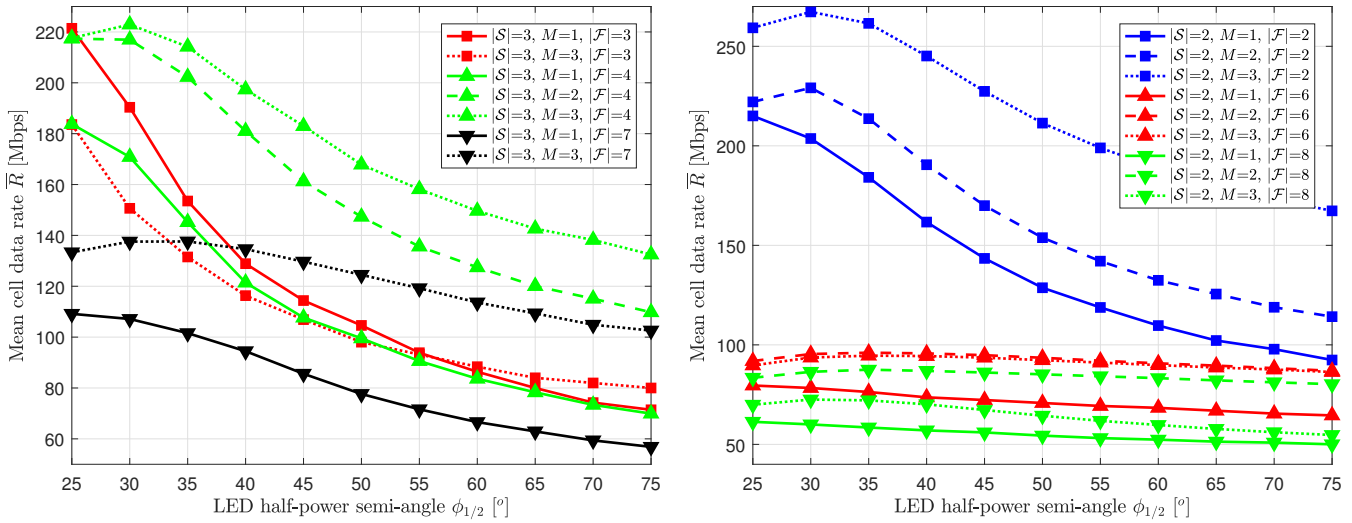

(a) RGB LEDs ($|C|$ = 3). (b) RGBY LEDs ($|C|$ = 4).

Fig. 12: Mean cell data rate $\overline{R}$ as function of angle $\phi_{1/2}$ when R = 1.5 m and different resource allocation configurations are used in stand-alone (M = 1) and cooperative ($M \geq 2$) modes. Blockage probability ρ_{block} = 40%.

considerable improvement when $\phi_{1/2}$ decreases (e.g., configurations with Q = 1 perform best with low $\phi_{1/2}$ values). Finally, we note that resource allocation configurations with Q = 3 and Q = 4 are the ones that perform best when $\phi_{1/2} \approx 25^\circ$ in RGB and $\phi_{1/2} \approx 30^\circ$ in RGBY, respectively. When moving beyond these LED half-power semi-angle thresholds, all the configurations degrade equally regardless of Q.

C. Performance of resource allocation configurations with cooperative transmission ($M \geq 2$)

Figs. 12a and 12b show the mean cell data rate as function of $\phi_{1/2}$ when stand-alone (M = 1) and cooperative ($M \geq 2$) transmission modes are used with resource allocation configurations that have $|\mathcal{S}|$ = 3 for RGB LEDs and $|\mathcal{S}|$ = 2 for RGBY LEDs, respectively. In all these cases, the blockage probability, which is the likelihood of having the LoS-link towards the nearest AP blocked in a given simulation instance, is set to ρ_{block} = 40%. Note that during a LoS-blockage event, the user will still receive optical signal power coming from the other (more distant) APs of the cooperating set. For simplicity, the blockage event is modeled as the outcome of an independent Bernoulli trial with probability p = 0.4. Note that the 4/3 gain observed when comparing the data rate with stand-alone transmission mode (M = 1) in case of both

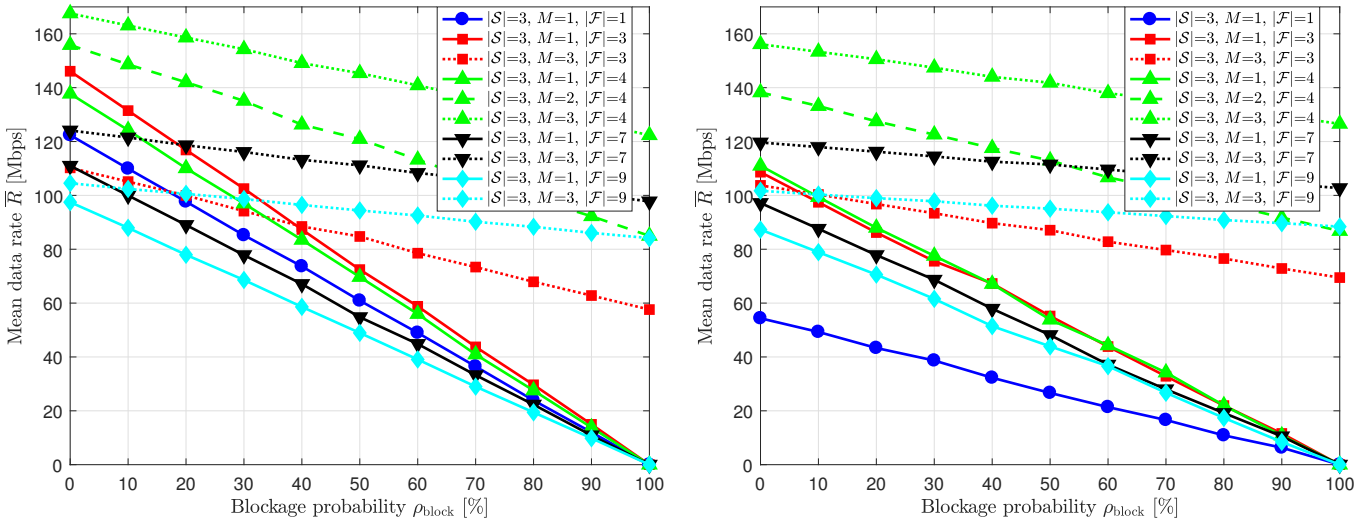

(a) Users located in the whole cell area

(b) Users located in the cell-edge area ($A_{\text{edge}} = 0.1\, A_{\text{cell}}$)

Fig. 13: Mean cell data rate $\overline{R}$ as function of the blockage probability ρ_{block} when RGB LEDs ($|C| = 3$), $R = 1.5$ m, $\phi_{1/2} = 60°$, and different resource allocation configurations for cooperative transmission with $|\mathcal{S}| = 3$ are used.

RGB and RGBY LEDs is not valid any more for cooperative transmission mode ($M \geq 2$). This is because all parameters of the resource allocation configurations used in cooperative transmission mode notably affect the achievable data rate, as the optical power allocated among the different sub-bands varies with the configuration that is being used. For both multi-color LEDs, when no cooperation is used ($M = 1$), the mean cell data rate is monotonically decreasing with $\phi_{1/2}$, and the best option is to select the most directional LED as long as the illumination requirements are verified (see Fig. 8). In contrast, when using a cooperative transmission mode ($M \geq 2$), an optimum LED semi-angle exists in data rate maximization sense. This is because very directional LEDs spread little optical power on adjacent cells; then, an optimum $\phi_{1/2}$ can be found, such that any increment beyond that threshold will decrease the data rate of the cooperative transmission, as a notable part of the optical power will become to be spread beyond the cooperating area. Note that the transmit power loss due to cooperation, as well as the high inter-cell interference level generated when $Q = 3$, become notable in the $\{|\mathcal{S}| = 3, |\mathcal{F}| = 3\}$ configuration, where the cooperative mode does not overcome the stand-alone (non-cooperative) mode up to a high $\phi_{1/2}$.

Finally, Figs. 13a and 13b show the mean data rate for users placed in the whole-cell area and cell-edge area, respectively. For the sake of brevity, these results are only obtained for RGB LEDs scenarios, as similar effects are observed when using RGBY LEDs. Note that the edge area of a cell is defined as the external ring, whose area is 10% of the area of the whole cell. As expected, the overall tendency is that cooperative transmission ($M \geq 2$) offers a better performance than non-cooperative ones ($M = 1$). Therefore, in schemes with low Q values (e.g., $Q = 3$), the cooperative transmission does not provide better performance than non-cooperative alternatives until a certain blockage probability is reached. Moreover, we have that blockage impacts more notably the configurations with low Q, as the inter-cell interference power that is present in these cases is larger. Thus, in scenarios with large ρ_{block}, it is better to use resource allocation configurations with large Q. As expected, users located on cell-edge areas are the most benefited due to the cooperation, since the data rate loss that they experience in case of blockage is negligible when compared to non-cooperative transmission cases. Besides, when studying the curves presented in Fig. 13a and Fig. 13b, it is possible to see that the mean data rate with cooperation is much more homogeneous distributed than with non-cooperative transmission.

V. Conclusion

This paper presented a thorough study of the different resource allocation configurations that can be applied in multi-cell VLC networks that implement (non-)cooperative transmission modes using multi-color LEDs in the APs. When designing these resource allocation patterns, an homogeneity requirement was sought to maintain the same spatial SINR statistics regardless of the sector of the VLC network under analysis. The different combinations of network configuration parameters that enable the desired SINR homogeneity requirement were clearly identified with the aid of statements. After that, the performance of these resource allocation configurations were evaluated in terms of LED type, number of frequency sub-bands per color, and number of sectors per cell. In addition, the working conditions were studied in detail to determine the transmission modes that comply with the illumination requirements. As expected, there is no single resource allocation configuration that performs best in all possible VLC network settings. Extensive simulation results were presented, demonstrating that, with a proper network

planning when allocating resources per AP, the mean cell data rate can be improved considerably. Besides, in presence of obstacles that may block the LoS link from AP to user, it was shown that the implementation of multi-point cooperative transmission modes is essential. Finally, it was observed that cooperative transmission also offers important gains in mean cell data rate, particularly when the LoS condition toward the serving VLC AP(s) can be guaranteed.

ACKNOWLEDGMENT

This work has been partially funded by the Spanish MECD FPU fellowship program granted to the author B. Genovés Guzmán, the Catalan Government under Grant 2017-SGR-1479, and the Spanish Government under the national project 'TERESA-ADA' with ID no. TEC2017-90093-C3-2-R and TEC2017-90093-C3-1-R (MINECO/AEI/FEDER, UE).

REFERENCES

[1] L. Hanzo, H. Haas, S. Imre, D. O'Brien, M. Rupp, and L. Gyongyosi, "Wireless myths, realities, and futures: from 3G/4G to optical and quantum wireless," *Proc. IEEE*, vol. 100, no. Special Centennial Issue, pp. 1853–1888, May 2012.

[2] Y. Wang, X. Wu, and H. Haas, "Load balancing game with shadowing effect for indoor hybrid LiFi/RF networks," *IEEE Trans. Wireless Commun.*, vol. 16, no. 4, pp. 2366–2378, Apr. 2017.

[3] H. Haas, "High-speed wireless networking using visible light," *SPIE Newsroom*, Apr. 2013.

[4] H. Haas, L. Yin, Y. Wang, and C. Chen, "What is LiFi?" *J. Lightw. Technol.*, vol. 34, no. 6, pp. 1533–1544, Mar. 2016.

[5] C. Chen, D. Tsonev, and H. Haas, "Joint transmission in indoor visible light communication downlink cellular networks," in *Proc. IEEE Globecom Workshops*, Dec. 2013, pp. 1127–1132.

[6] C. Chen and H. Haas, "Performance evaluation of downlink cooperative multipoint joint transmission in LiFi systems," in *Proc. IEEE Globecom Workshops*, Dec. 2017, pp. 1–6.

[7] C. Chen, S. Videv, D. Tsonev, and H. Haas, "Fractional frequency reuse in DCO-OFDM-based optical attocell networks," *J. Lightw. Technol.*, vol. 33, no. 19, pp. 3986–4000, Oct. 2015.

[8] H. Kazemi and H. Haas, "Downlink cooperation with fractional frequency reuse in DCO-OFDMA optical attocell networks," in *Proc. IEEE International Conference on Communications*, May 2016, pp. 1–6.

[9] V. Jungnickel, K. Manolakis, W. Zirwas, B. Panzner, V. Braun, M. Lossow, M. Sternad, R. Apelfrojd, and T. Svensson, "The role of small cells, coordinated multipoint, and massive MIMO in 5G," *IEEE Commun. Mag.*, vol. 52, no. 5, pp. 44–51, May 2014.

[10] R. Irmer, H. Droste, P. Marsch, M. Grieger, G. Fettweis, S. Brueck, H. Mayer, L. Thiele, and V. Jungnickel, "Coordinated multipoint: Concepts, performance, and field trial results," *IEEE Commun. Mag.*, vol. 49, no. 2, pp. 102–111, Feb. 2011.

[11] A. Dowhuszko and A. Pérez-Neira, "Achievable data rate of coordinated multi-point transmission for visible light communications," in *Proc. IEEE Int. Symp. Personal, Indoor, and Mobile Radio Commun.*, Oct. 2017, pp. 1–7.

[12] H. Ma, L. Lampe, and S. Hranilovic, "Coordinated broadcasting for multiuser indoor visible light communication systems," *IEEE Trans. Commun.*, vol. 63, no. 9, pp. 3313–3324, Sept. 2015.

[13] H. Ma, A. Mostafa, L. Lampe, and S. Hranilovic, "Coordinated beamforming for downlink visible light communication networks," *IEEE Trans. Commun.*, vol. 66, no. 8, pp. 3571–3582, Aug. 2018.

[14] M. Demir, F. Miramirkhani, and M. Uysal, "Handover in VLC networks with coordinated multipoint transmission," in *Proc. IEEE International Black Sea Conference on Communications and Networking*, June 2017, pp. 1–5.

[15] L. Yin, X. Wu, H. Haas, and L. Hanzo, "Low-complexity SDMA user-grouping for the CoMP-VLC downlink," in *Proc. IEEE Global Communications Conference*, Dec. 2015, pp. 1–6.

[16] B. Guzmán, A. Serrano, and V. Jiménez, "Cooperative optical wireless transmission for improving performance in indoor scenarios for visible light communications," *IEEE Trans. Consum. Electron.*, vol. 61, no. 4, pp. 393–401, Nov. 2015.

[17] B. Guzmán, A. Dowhuszko, V. Jiménez, and A. Pérez-Neira, "Robust cooperative multicarrier transmission scheme for optical wireless cellular networks," *IEEE Photon. Technol. Lett.*, vol. 30, no. 2, pp. 197–200, Jan. 2018.

[18] B. Guzmán, A. Dowhuszko, V. Jiménez, and A. Pérez-Neira, "Cooperative transmission scheme to address random orientation and blockage events in VLC systems," in *Proc. Int. Symp. Wireless Commun. Syst.*, Aug. 2019, pp. 351–355.

[19] T. Qiu, N. Chen, K. Li, M. Atiquzzaman, and W. Zhao, "How can heterogeneous internet of things build our future: A survey," *IEEE Commun. Surveys Tuts.*, vol. 20, no. 3, pp. 2011–2027, 2018.

[20] H. Chun, S. Rajbhandari, G. Faulkner, D. Tsonev, E. Xie, J. McKendry, E. Gu, M. Dawson, D. O'Brien, and H. Haas, "LED based wavelength division multiplexed 10 Gb/s visible light communications," *J. Lightw. Technol.*, vol. 34, no. 13, pp. 3047–3052, July 2016.

[21] Y. Wang, L. Tao, X. Huang, J. Shi, and N. Chi, "8-Gb/s RGBY LED-based WDM VLC system employing high-order CAP modulation and hybrid post equalizer," *IEEE Photon. J.*, vol. 7, no. 6, pp. 1–7, Dec. 2015.

[22] C. Chen, D. A. Basnayaka, and H. Haas, "Downlink performance of optical attocell networks," *J. Lightw. Technol.*, vol. 34, no. 1, pp. 137–156, Jan. 2016.

[23] Z. Wang, Q. Wang, W. Huang, and Z. Xu, *Visible light communications: modulation and signal processing*. Wiley-IEEE Press, 2018.

[24] S. Dimitrov, S. Sinanovic, and H. Haas, "Clipping noise in OFDM-based optical wireless communication systems," *IEEE Trans. Commun.*, vol. 60, no. 4, pp. 1072–1081, Apr. 2012.

[25] Y. Zhuang, L. Hua, L. Qi, J. Yang, P. Cao, Y. Cao, Y. Wu, J. Thompson, and H. Haas, "A survey of positioning systems using visible LED lights," *IEEE Commun. Surveys Tuts.*, vol. 20, no. 3, pp. 1963–1988, 2018.

[26] J. M. Kahn and J. R. Barry, "Wireless infrared communications," *Proc. IEEE*, vol. 85, no. 2, pp. 265–298, Feb. 1997.

[27] T. Komine and M. Nakagawa, "Fundamental analysis for visible-light communication system using LED lights," *IEEE Trans. Consum. Electron.*, vol. 50, no. 1, pp. 100–107, Feb. 2004.

[28] B. Guzmán, V. Jiménez, M. Aguayo-Torres, H. Haas, and L. Hanzo, "Downlink performance of optical OFDM in outdoor visible light communication," *IEEE Access*, vol. 6, pp. 76 854–76 866, Nov. 2018.

[29] *Light and Lighting-Lighting of work places-Part 1: Indoor work places*, European Std. EN 12 464-1, June 2011.

[30] T. Rappaport, *Wireless communications: Principles and practice*, 2nd ed., ser. Prentice Hall communications engineering and emerging technologies series. Prentice Hall, 2002.

[31] B. Almeroth, A. Fehske, G. Fettweis, and E. Zimmermann, "Analytical interference models for the downlink of a cellular mobile network," in *Proc. IEEE Globecom Workshops*, Dec. 2011, pp. 739–743.

Borja Genovés Guzmán (S'14) received his B.Sc. from the University Carlos III of Madrid in 2013, and a double M.Sc. degree in electrical engineering from the University Carlos III of Madrid and the Institut Mines-Télécom (France) in 2015, both with honours. He received the First prize in Graduation National Awards by the Ministry of Education, Culture and Sports of Spain. He received the Ph.D. degree from the University Carlos III of Madrid in 2019. He was a visiting scholar in the Southampton Wireless Group at The University of Southampton and in the LiFi Research and Development Centre at The University of Edinburgh, in 2017 and 2018, respectively. He was a recipient of an FPU scholarship from the Spanish Ministry of Education, Culture and Sports of Spain. He has participated in several national and European projects. He is currently a post-doc researcher at IMDEA Networks Institute. His current research focuses on new techniques to improve the efficiency of optical wireless communications systems, next generation wireless networks and mobile communications.

Alexis Dowhuszko (M'13, SM'18) received the Telecommunications Engineering degree from Blas Pascal University, Cordoba, Argentina, in 2002, and the PhD degree in Engineering Sciences from the National University of Cordoba, Argentina, in 2010. From 2010 to 2015, he was a Postdoc Researcher at the Department of Communications and Networking, Aalto University, Finland. In early 2016, he moved to Spain to take a Senior Researcher position at the Centre Tecnològic de les Telecomunicacions de Catalunya (CTTC), Barcelona. He returned to Aalto University in Aug. 2020, to take a Research Fellow position at the Department of Communications and Networking. His areas of interest focus on disruptive communication concepts, technologies, and architectures for 5G and beyond, including wireless communications beyond mmWave frequency bands (VLC, FSO, and Terahertz), integration of radio and optical technologies in High-Throughput Satellite systems, and use of Artificial Intelligence for the autonomous operation of Wireless Networks.

Víctor P. Gil Jiménez (S'00, AM'02, M'03, SM'12) received the B.S and the M.S in Telecommunication degree in 1998 and 2001, from the University of Alcalá and University Carlos III of Madrid, respectively, and the PhD. degree in 2005 from the University Carlos III of Madrid, all of them with Honors. He is with the department of Signal Theory and Communications at the University Carlos III of Madrid as Associate Professor. He worked at the Spanish Antarctica Base in 1999 as Communications Staff. He visited University of Leeds (UK), Chalmers Technical University (Sweden) and Instituto de Telecommunicaçoes (Portugal) in 2003, 2004 and 2008 - 2010, respectively. He has also led several private and national Spanish projects and has participated in several European and international projects. He holds one patent. He has received the Master Thesis and a PhD Thesis Award by the Professional Association of Telecommunication Engineers of Spain in 1998 and 2006, respectively. He has published over 50 journal/conference papers and 7 book chapters. His interests are in the field of the advanced multicarrier systems for wireless radio and visible light communications. He held the IEEE Spanish Communications and Signal Processing Joint Chapter chair (2015 - 2020).

Ana Pérez-Neira (SM'02, FM'20) is full professor at Universitat Politècnica de Catalunya in the Signal Theory and Communication department since 2006 and was Vice rector for Research (2010-14). She is fellow researcher at Centre Tecnològic de Telecomunicacions de Catalunya, where she is the Coordinator of the SatCom and Space activities. Her research is in signal processing for communications, focused on satellite communications. She has more than 60 journal papers and 300 conference papers. She is co-author of 7 books. She has leaded more than 20 projects and holds 8 patents. She is the coordinator of the Network of Excellence on satellite communications, financed by the European Space Agency: SatnexIV. She has been associate editor of the IEEE TSP and EURASIP SP and ASP. Currently she is senior area editor of OJSP. She is member of the BoG of the IEEE SPS. She is IEEE Fellow and member of the Real Academy of Science and Arts of Barcelona (RACAB). She is recipient for the 2018 EURASIP Society Award and she is the general chair of IEEE ICASSP'20.